Diffusion of Oxygen, Nitrogen and Their Mixtures in Carbon Molecular Sieve

Y. D. Chen, R. T. Yang, and P. Uawithya
Dept. of Chemical Engineering, State University of New York at Buffalo, Buffalo, NY 14260

Diffusivities of oxygen, nitrogen and their mixtures in carbon molecular sieve are measured under conditions used for kinetic separation of air by adsorption (elevated pressures). In binary diffusion, codiffusion enhances fluxes for both components, whereas counterdiffusion has the opposite effects; for both cases, the effects are significantly more pronounced for the fast diffusing component. The multicomponent diffusion theory developed earlier in this laboratory for surface diffusion is reformulated for diffusion in molecular sieves. Multicomponent diffusivities can be predicted from the following pure-component information: concentration-dependent diffusivities and diffusional activation energies. Predicted binary diffusion results agree fairly with the experimental data for oxygen and nitrogen in carbon molecular sieve.

Introduction

Carbon molecular sieve (CMS) is a unique class of material with pore sizes in the range of 3-5 Å and is being used for the production of nitrogen from air by pressure swing adsorption (PSA) (Yang, 1987). This is the only major application of kinetic separation by adsorption, that is, separation caused by differences in molecular diffusivities in the microporous structure of the sorbent. Understanding this process requires knowledge on both equilibrium and diffusion of mixtures of oxygen and nitrogen in the sorbent. Moreover, since this PSA separation process is normally operated in the pressure range 1-7 atm (Yang, 1987), information at elevated pressures is needed.

Considerable pure-component diffusivity and equilibrium adsorption data of oxygen and nitrogen on CMS are available (Kawazoe et al., 1974; Knoblauch, 1978; Chihara et al., 1978; Ruthven et al., 1986; Dominguez et al., 1988; La Cava et al., 1989; Ruthven, 1992). All of these studies, however, were limited to pure component and 1-atm pressure. The first objective of this study was to gather information on the diffusivities of oxygen, nitrogen and their *mixtures* at elevated pressures: up to 12 atm for pure-component diffusion and 5 atm for binary diffusion.

Despite the voluminous literature on diffusion in zeolite molecular sieves, studies on multicomponent diffusion are relatively few and our knowledge on the subject remains primitive (Habgood, 1958; Ma and Roux, 1973; Karger et al., 1975; Karger and Bulow, 1975; Ma and Lee, 1977; Ruthven and Kumar, 1979; Palekar and Rajadhyaksha, 1986; Marutovsky and Bulow, 1987; Yasuda and Matsumoto, 1989; Krishna, 1990; Qureshi and Wei, 1990a,b; Tsikoyiannis and Wei, 1991a,b; Yang et al., 1991; Chen and Yang, 1992; Nelson and Wei, 1992; Chen et al., 1993; Krishna, 1993). There are only few theories with which one can predict multicomponent diffusivities from pure-component diffusivities, as discussed by Chen and Yang (1992). The theory of Chen and Yang (1992) was derived for surface diffusion, but is also applicable to diffusion in molecular sieves, which will be explained shortly. This theory is simple to use and requires only concentration-dependent pure-component diffusivities and diffusional activation energies. The second objective of this study was to test this theory for the binary diffusion system O_2/N_2/CMS.

Experimental Studies

The carbon molecular sieve sample was manufactured by Bergbau-Forschung GmbH in Germany (Yang, 1987). The Bergbau-Forschung CMS and similar materials are widely used for N_2 production. Unlike zeolite molecular sieve, which has a discrete, crystalline pore structure, the CMS has a pore size distribution between approximately 3 to 5 Å. Pellets of the

Correspondence concerning this article should be addressed to R. T. Yang.

sample with sizes between 2-3 mm were used in the experiments. Each pellet was composed of many small crystals. The size distribution of the crystals was measured by electron microscopy. The samples were degassed *in vacuo* at 90°C for approximately 12 hours before each diffusion experiment.

The differential adsorption bed (DAB) technique was used for measuring diffusivities. The technique was first used by Habgood (1958) and further developed and refined by Carlson and Dranoff (1987) and Do et al. (1991). This is a versatile technique capable of providing simultaneously equilibrium and diffusivity data for both single component and gas mixtures. In this technique, the adsorptive gas is passed through a differential bed of adsorbent pellets. The gas velocity is high enough to assure isothermal adsorption, and the inlet and outlet concentrations of gas phase are equal. The experiment is initiated by making a step change in the adsorptive concentration in the feed stream. The DAB is exposed to the feed stream for a finite period of time after the step change in feed concentration. At the end of this exposure period, the adsorbates are thermally desorbed into a collecting vessel of known volume and analyzed to determine the total amount and composition of the adsorbates. By varying the periods of exposure, adsorption rate data can be obtained. Since this method is carried out under differential conditions, it can be operated under high pressure and has the advantage that the associated mathematical analysis is much simplified.

The DAB used in this work was constructed from a 3/8-in. (9.5-mm) stainless-steel Cajon plug. The sorbent was supported on a 100-μm stainless-steel mesh. An 1/8-in. (3.2-mm) type K thermocouple was located axially within the bed to measure the sorbent temperature. A 12-in. (305-mm) Bourdon pressure gauge, spanning 1,000 psig (6.9 MPa) in 1-psig (6.9-kPa) increments, was used to indicate the sorption pressure. The adsorber temperature was controlled by 1/2-in. (12.7-mm)-wide Thermolyne flexible electric heating tape. The bed contained 2.5075 g of 2-3-mm-dia. Bergbau-Forschung carbon molecular sieve pellets.

The experimental procedure varied slightly depending on whether the experiment involved adsorption or desorption and whether it involved one or two sorbates. For the single-component adsorption rate experiment, the DAB was initially pressurized with helium and then isolated. The single-component gas, with 10-15% of O_2 or N_2 and helium as the inert, was premixed and passed through the DAB for a designated exposure time at the same pressure as the isolated helium and at a high flow rate. The DAB was then isolated, and the temperature was increased to 75°C. Desorption into the desorption vessel was allowed for at least 3 h. From the pressure, the amount of adsorbate was determined. For high partial pressure diffusion data, the DAB was preequilibrated with 85-90% of O_2 or N_2 at a designated pressure. Then, the pure diffusing gas was passed through the DAB for a period of time under the same diffusion pressure. Following the same desorption procedure, one can obtain the high-pressure diffusion data.

To simulate the air separation system, most of the binary diffusion experiments were conducted with mixtures containing N_2/O_2 ratio near that of air. The experimental procedure is similar to the high-pressure single-component diffusion experiment except that the desorbed gas was also analyzed by GC to determine the adsorbed-phase composition.

To test if the macropore (intercrystal, intrapellet) diffusional resistance was significant, an experiment involving uptake rates under identical conditions for two different pellet sizes of adsorbent was performed. In this case, only adsorption rate of pure nitrogen at 25°C was considered. Uptake curves for both cases are compared in Figure 1. It is apparent that the rate of sorption for the crushed CMS pellets (0.050-0.084 mm sizes) was very similar to that of the full-size (2-3 mm) pellets. This indicates that the resistances in the macropores were small compared to those in micropores. Therefore, it can be concluded that the diffusion process was controlled by intracrystalline diffusion.

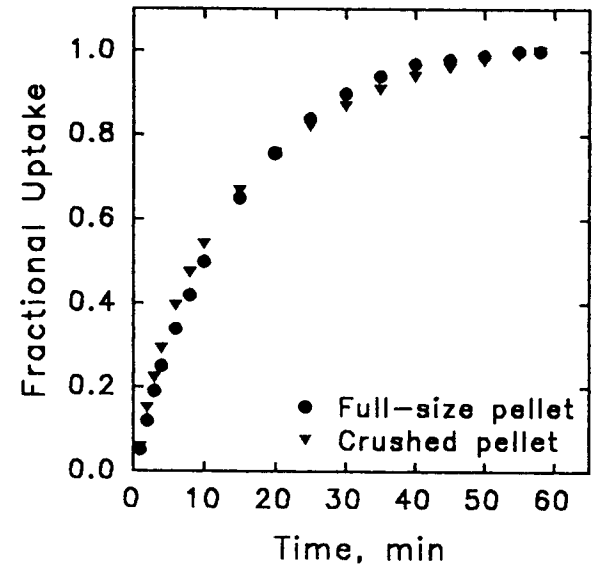

Figure 1. Pure gas fractional uptake of N_2 on Bergbau-Forschung carbon molecular sieve at 25°C.

In Figure 1, N_2 diffusion was slightly faster in the crushed pellets during the initial stage. This was consistent with the well known "skin effect" reported in the literature for extruded pellets of zeolites, where the skin offers an additional diffusional barrier. After the initial stage, a slightly faster uptake was observed for the full-size pellets. This was apparently caused by the small temperature rise within the full-size pellets even though the gas-phase temperatures were the same for both cases; a very small temperature rise could account for the slightly higher diffusion rate in Figure 1.

The isothermal diffusion condition was implied by the thermocouple reading with the thermocouple outside the pellets. To assure that the isothermal condition was indeed valid, a conservative energy balance was made in which the heat of adsorption was assumed to completely convert to temperature rise in the pellet. A 5.54×10^{-7} mmol uptake of O_2 by a 0.0135-g pellet generated approximately 8.58×10^{-6} kJ (based on the experimental data on heat of adsorption, 1 cal = 4.1868 J). Using the heat capacity of 0.25 cal/g/°C for CMS, the maximum temperature rise in the pellet would be 0.6°C. The isothermal condition was thus verified.

Results and Discussion

Microparticle-size distribution

The molecular sieve carbon pellet was composed of crystalline microparticles (Chihara et al., 1978). The size distri-

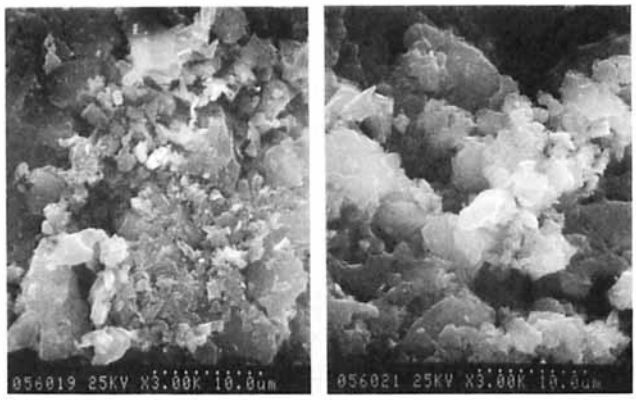

Figure 2. Bergbau-Forschung CMS pellets.

bution of the Bergbau CMS was determined by scanning electron microscopy (SEM). The pellets were dissected, and samples of the SEM pictures of the cross-sectional surfaces are shown in Figure 2. The dimensions of approximately 300 microparticles were measured from the SEM pictures. The size distribution was found to follow approximately a log-normal distribution (Irani and Callis, 1963):

$$f(R)=\frac{1}{\sqrt{2\pi}\ln\sigma}\exp\left(-\left[\frac{\ln(R/R_0)}{\sqrt{2}\ln\sigma}\right]^2\right) \quad (1)$$

where R is radius, R_0 is geometric mean radius on a volume fraction basis and σ is the geometric standard deviation. The relationship between the geometric mean radius on a number fraction basis, (R_0'), and on a volume fraction basis (R_0) is (Irani and Callis, 1963):

$$R_0=R_0'\exp[3(\ln\sigma)^2] \quad (2)$$

For log-normal distribution, a plot of the cumulative volume fraction (the integral of Eq. 1) against log R should yield a straight line. Moreover, such a "log-normal" plot on a number fraction basis and that on a volume fraction basis should both yield straight lines which are parallel.

From the SEM data, the cumulative number fraction was plotted against the microparticle radius in the log-normal fashion, as shown in Figure 3. A straight line was obtained, confirming the log-normal distribution. The geometric mean radius on a volume fraction basis (R_0) was 4.31 μm: the standard deviation (σ) was 2.15 and the geometric mean radius on a number fraction basis (R_0') was 0.74 μm.

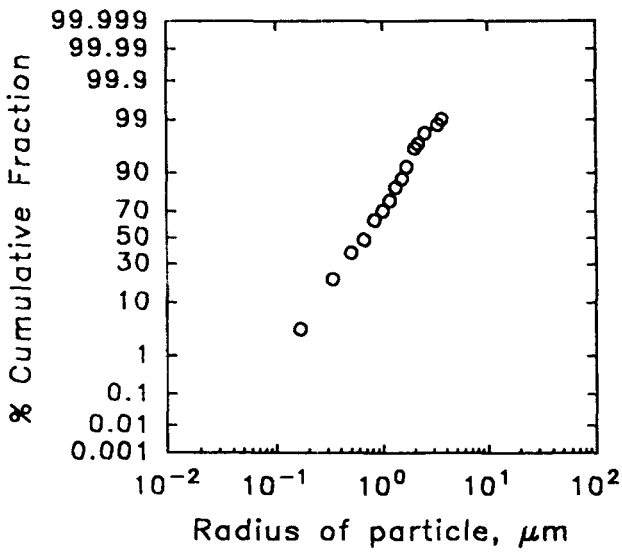

Figure 3. Log-normal size distribution of the microparticles of Bergbau-Forschung CMS.

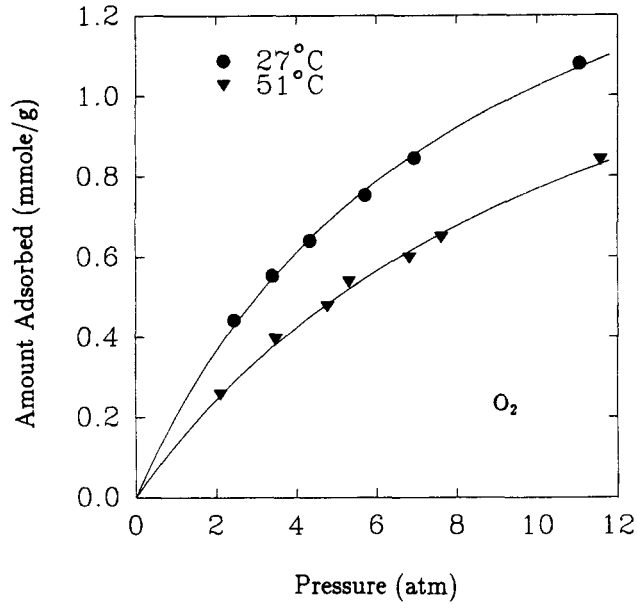

Figure 4. Equilibrium isotherm of oxygen on CMS.

Equilibrium isotherms

The equilibrium isotherms for O_2 and N_2 on the Bergbau

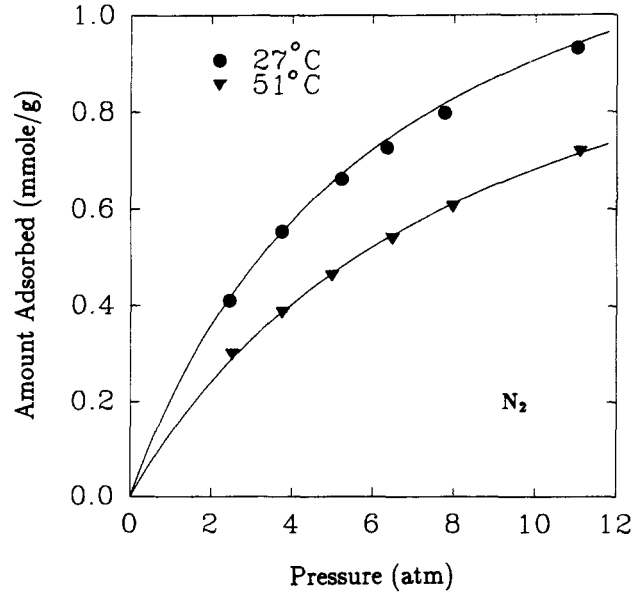

Figure 5. Equilibrium isotherm of nitrogen on CMS.

Table 1. Pure-Component Equilibrium (Langmuir Isotherm, Eq. 3) and Diffusion (Eq. 5) Data in CMS*

Comp.	Temp.	q_s (mmol/g)	b (1/atm)	D_0/R^2 (1/s)	λ	ϵ, kcal/mol
O_2	27°C	1.874	0.1204	3.478×10^{-4}	5.282×10^{-2}	5.585
	51°C	1.679	0.0842			
N_2	27°C	1.469	0.1614	9.514×10^{-6}	1.287×10^{-2}	6.851
	51°C	1.260	0.1179			

*Diffusional Activation Energies (ϵ) are taken from Kikkinides and Yang (1993).

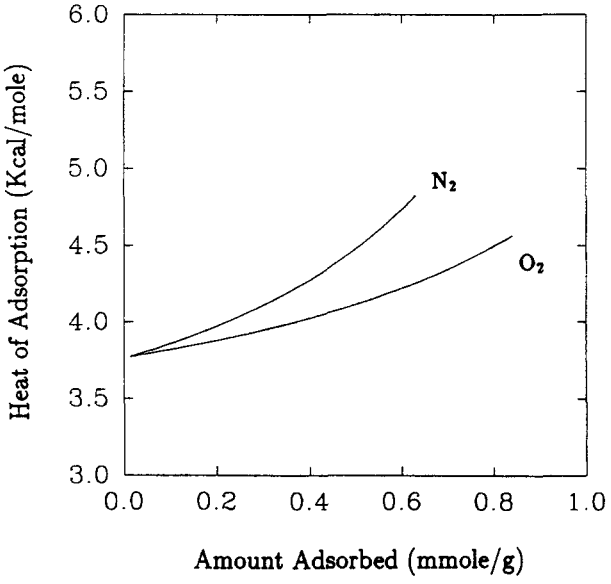

Figure 6. Isosteric heats of adsorption on CMS.

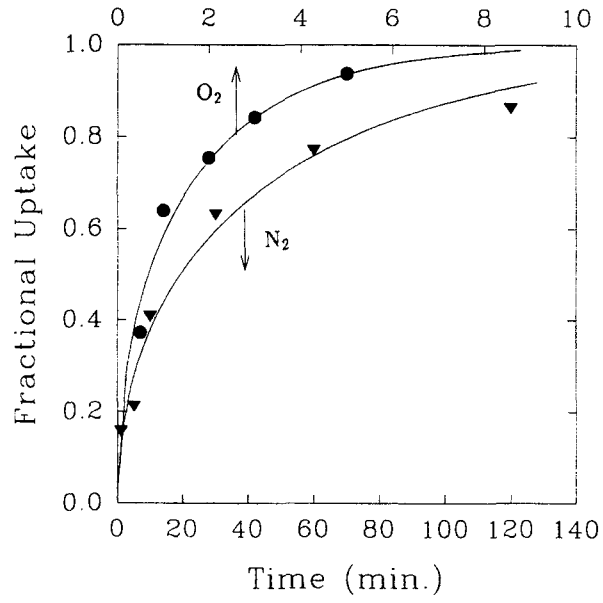

Figure 7. Uptake amounts at different time lengths for O_2 and N_2 in CMS at 27°C.

Each point is taken separately from time zero.

CMS in the pressure range 0–12 atm and at two temperatures, 27 and 51°C, are shown in Figures 4 and 5.

The equilibrium data can be fitted well by the Langmuir isotherm:

$$q=\frac{q_s bP}{1+bP} \tag{3}$$

The fitting parameters are listed in Table 1. The isosteric heats of adsorption were calculated from the temperature dependence and are shown as functions of amount adsorbed in Figure 6. The slightly increasing heats of adsorption indicated the absence of energetic heterogeneity and the presence of lateral interactions.

Six sets of binary O_2/N_2 equilibrium adsorption data are also available from the diffusion experiments. The equilibrium data are given in Table 2. Because of the scarcity of the equilibrium data and the narrow range of composition, no attempt was made to correlate these data.

Single-component, concentration-dependent diffusivities

Figure 7 shows the uptake rates of O_2 and N_2 in CMS at 27°C measured by the DAB technique. These uptake rates

Table 2. Initial and Final States for Binary Diffusion Experiments at 27°C*

Total Pres. (atm)	Initial Amounts Adsorbed		Final Amounts Adsorbed		Corresp. Figures
	$q_{O_2}\times10^4$(mol/g)	$q_{N_2}\times10^4$ (mol/g)	$q_{O_2}\times10^4$ (mol/g)	$q_{N_2}\times10^4$ (mol/g)	
3.700	2.4418 (0.3984)**	2.9268 (0.6016)	1.4027 (0.2159)	3.9187 (0.7841)	Fig. 11
5.106	2.1387 (0.2159)	4.7088 (0.7841)	1.6895 (0.1926)	4.4595 (0.6700)	Fig. 12
5.078	1.7182 (0.1922)	4.0515 (0.6740)	2.1293 (0.2159)	4.6996 (0.7841)	Fig. 13
5.066	1.0190 (0.1191)	5.2595 (0.8809)	2.1388 (0.2159)	4.7041 (0.7841)	Fig. 14
5.009	0 (0)	0 (0)	1.9635 (0.2159)	4.8815 (0.7841)	Fig. 15
5.036	7.0455 (1.0)	0 (0)	1.9639 (0.2159)	4.8116 (0.7841)	Fig. 16

*The amounts adsorbed (q) are equilibrium values.
**Quantities in parentheses are gas-phase mole fractions.

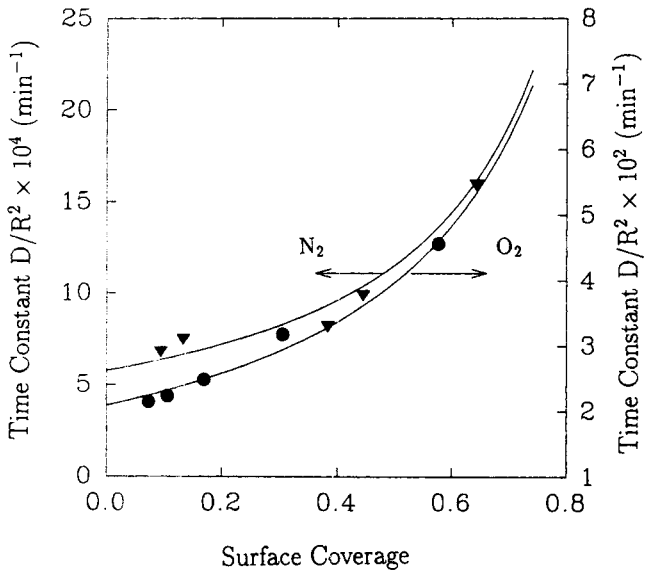

Figure 8. Concentration dependence of diffusional time constants for oxygen and nitrogen at 27°C.

were measured at a constant pressure (11.295 atm) with small increments in concentration. In this manner, the concentration-dependent diffusivities could be determined. The diffusional time constants, D/R^2, were calculated from the incremental uptake rates from the solution of the diffusion equation:

$$\frac{q}{q_\infty} = 1 - \frac{6}{\pi^2} \sum_{n=1}^{\infty} \frac{1}{n^2} e^{-\pi^2 n^2 Dt/R^2} \tag{4}$$

The values of D/R^2 were obtained by nonlinear regression using the least-square method.

The diffusion time constants for both O_2 and N_2 were strongly concentration-dependent, as shown in Figure 8. The concentration dependence was fitted by (Chen and Yang, 1992):

$$D = D_0 \frac{1}{1-(1-\lambda)\theta} \tag{5}$$

where θ is the fractional amount adsorbed based on the maximum amount in the Langmuir isotherm, and λ is a fitting parameter, the meaning of which will be given shortly. The values of λ and D_0 are also listed in Table 1, along with pure-component equilibrium data.

Due to the industrial importance of the Bergbau CMS, diffusion measurements have been reported by a number of groups. Compared to the data in the literature, our data appeared to be at the lower end. This comparison prompted us to examine different conditions under which the carbon samples were pretreated by different groups before diffusion measurements. The "activation" temperature of 300–350°C is generally employed for zeolite samples. For carbon samples, however, appreciable oxidation/gasification could occur at these temperatures (Walker et al., 1959). Moreover, oxidation in this temperature range is generally kinetically controlled, resulting in uniform enlargement of the pores (Walker et al., 1959). The diffusivity data for CMS samples "activated" at 90°C and 350°C are compared in Table 3. The diffusivities differed by over an order of magnitude. The gas atmosphere employed for activation was helium at 99.995% minimum purity. Activation at 350°C in this helium atmosphere resulted in a weight loss for the CMS of 3.6%. The corresponding N_2 adsorption (at 27°C) increased, in the q_s (see Eq. 3) amount, from 2.61 mg/g to 3.36 mg/g as a result of the higher pretreatment temperature. Based on these results, the higher diffusivities in the CMS pretreated at 350°C were attributed to the enlargement of the pores due to carbon gasification. It is thus speculated that the higher diffusivities in the literature (also included in Table 3) were possibly caused by their higher pretreatment temperatures.

Predicting multicomponent diffusivities from pure-component diffusivities for diffusion in molecular sieve (zeolite or carbon)

Two predictive theories have been formulated for predicting multicomponent Fickian diffusivities from pure-component data (Yang et al., 1991; Chen and Yang, 1992). The first one was derived from principles of irreversible thermodynamics, which requires mixed-gas isotherms (or their implicit forms), $P_i(q_1, q_2 \ldots\ldots q_n)$, to account for the mixed-adsorbate interactions (Yang et al., 1991; Chen et al., 1993). In the second theory, a simple solution was derived based on kinetic theory. This theory was formulated for surface diffusion, but can be also applied to diffusion in zeolite as discussed below.

The multicomponent flux equation is given by:

$$\vec{J} = -[D]\nabla\vec{q} \tag{6}$$

where $\vec{J}$ and $\vec{q}$ are two vectors of n components, respectively, for flux and adsorbate concentration. The multicomponent diffusivity matrix $[D]$ is given by (Chen and Yang, 1992; Chen et al., 1993):

Table 3. Comparison of Pure-Component Diffusivities in Bergbau Carbon Molecular Sieve

Temp. (K)	Method	Pretreatment	D_{O_2}/R^2 (1/s)	D_{N_2}/R^2 (1/s)	Reference
300	DAB	vac., 90°C	3.5×10^{-4}	9.5×10^{-6}	This work
300	Gravimetric	He, 90°C	3.6×10^{-4}	1.6×10^{-5}	Kikkinides/Yang (1993)
300	Gravimetric	He, 350°C		1.86×10^{-4}	This work
300	Volumetric		1.7×10^{-4}	7.0×10^{-6}	Knoblauch (1978)
300	Gravimetric	250–300°C	3.5×10^{-3}	1.1×10^{-4}	Ruthven et al. (1986)
300	Gravimetric	He, 200°C	2.3×10^{-3}	6.0×10^{-5}	Farooq/Ruthven (1991)
273	Gravimetric	vac., 250°C	2.4×10^{-4}	3.5×10^{-6}	Ruthven (1992)

$$D_{ii} = D_{io} \frac{\left[1 - \sum_{j=1}^{n} (1 - \lambda_{ij})\theta_j\right]_{j \neq i}}{1 - \sum_{j=1}^{n} (1 - \lambda_{ij})\theta_j} \tag{7}$$

$$D_{ij} = D_{io} \frac{[(1 - \lambda_{ij})\theta_i]_{j \neq i}}{1 - \sum_{j=1}^{n} (1 - \lambda_{ij})\theta_j} \tag{8}$$

For binary diffusion of components A and B, the fluxes are:

$$J_A = -D_{AA} \frac{\partial q_A}{\partial x} - D_{AB} \frac{\partial q_B}{\partial x} \tag{9}$$

$$J_B = -D_{BA} \frac{\partial q_A}{\partial x} - D_{BB} \frac{\partial q_B}{\partial x} \tag{10}$$

and the concentration-dependent Fickian diffusivities are:

$$D_{AA} = D_{AO}\left[\frac{1 - (1 - \lambda_{AB})\theta_B}{1 - (1 - \lambda_A)\theta_A - (1 - \lambda_{AB})\theta_B}\right] \tag{11}$$

$$D_{AB} = D_{AO}\left[\frac{(1 - \lambda_{AB})\theta_A}{1 - (1 - \lambda_A)\theta_A - (1 - \lambda_{AB})\theta_B}\right] \tag{12}$$

$$D_{BA} = D_{BO}\left[\frac{(1 - \lambda_{BA})\theta_B}{1 - (1 - \lambda_B)\theta_B - (1 - \lambda_{BA})\theta_A}\right] \tag{13}$$

$$D_{BB} = D_{BO}\left[\frac{1 - (1 - \lambda_{BA})\theta_A}{1 - (1 - \lambda_B)\theta_B - (1 - \lambda_{BA})\theta_A}\right] \tag{14}$$

where D_{AO} and D_{BO} are pure-component diffusivities at zero coverage, given by (for D_{AO}):

$$\frac{D_A}{D_{AO}} = \frac{1}{1 - (1 - \lambda_A)\theta_A} \tag{15}$$

Since the values of q_s for the two components are not very different, one may adopt the adsorbed-phase averaging scheme of Innes et al. (Chapter 3, Yang, 1987) for calculating q_s:

$$\frac{1}{q_s} = \frac{X_A}{q_{sA}} + \frac{X_B}{q_{sB}} \tag{16}$$

and

$$\theta_A = \frac{q_A}{q_s},\ \theta_B = \frac{q_B}{q_s},\ \theta_A + \theta_B \leq 1 \tag{17}$$

where X is the adsorbed-phase mole fraction at equilibrium.

The parameter λ reflects the difference between the effective bond energy of molecule A and vacant site (ϵ_{AV}) and that of molecule A on a site already occupied by A(ϵ_{AA}) (Yang et al., 1973):

$$\lambda_A = \frac{\text{sticking probability on adsorbed } A}{\text{sticking probability on vacant site}} = e^{-(\epsilon_{AV} - \epsilon_{AA})/RT} \tag{18}$$

Similarly,

$$\lambda_B = e^{-(\epsilon_{BV} - \epsilon_{BB})/RT} \tag{19}$$

$$\lambda_{AB} = e^{-(\epsilon_{AV} - \epsilon_{AB})/RT} \tag{20}$$

$$\lambda_{BA} = e^{-(\epsilon_{BV} - \epsilon_{BA})/RT} \tag{21}$$

For surface diffusion, we have assumed ϵ_{AV} and ϵ_{BV} to be heats of adsorption (Chen and Yang, 1992). For diffusion in zeolite, the derivation is also valid, provided that the activation energies for diffusion are used for ϵ_{AV} and ϵ_{BV}. In contrast to surface diffusion, in which the activation energy is always lower than the heat of adsorption, the activation energy for diffusion in zeolite can be higher than heat of adsorption, because the repulsive forces between the diffusing molecule and the aperture or pore surfaces can dominate the diffusion process.

From the experimental values of λ_A and ϵ_{AV}, the value for ϵ_{AA} can be obtained from Eq. 18. Finally, the interaction energies between unlike molecules, ϵ_{AB} or ϵ_{BA}, can be calculated by assuming the mixing rule:

$$\epsilon_{AB} = \epsilon_{BA} = (\epsilon_{AA}\epsilon_{BB})^{1/2} \tag{22}$$

Binary diffusion results and comparison with theory

The DAB technique was employed to measure binary diffusion of O_2/N_2 in Bergbau CMS in the total pressure range 3.7-5.066 atm at 27°C. Six sets of measurements were made with the initial and final equilibrium conditions in Table 2. These included three sets for codiffusion and three sets for counterdiffusion. The experimental results are shown in Fig-

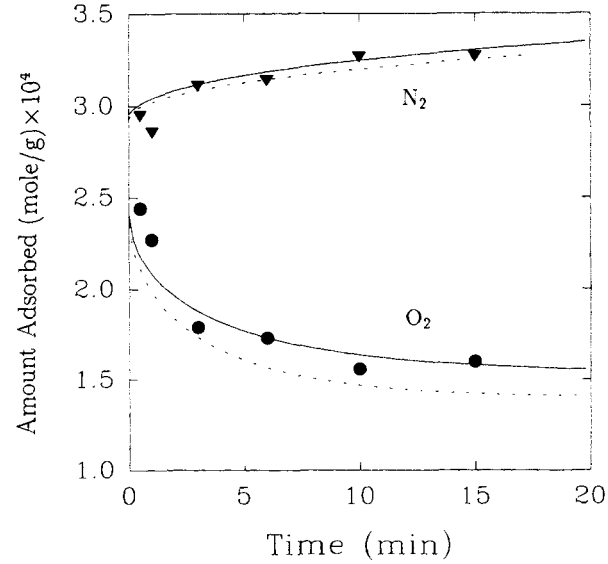

Figure 9. Counterdiffusion of N_2 and O_2 in CMS at 27°C.

Symbols are experimental data. Curves are predictions using pure-component diffusivities (· · · ·) and theoretical binary diffusivities (——). See Table 3 for initial and final conditions.

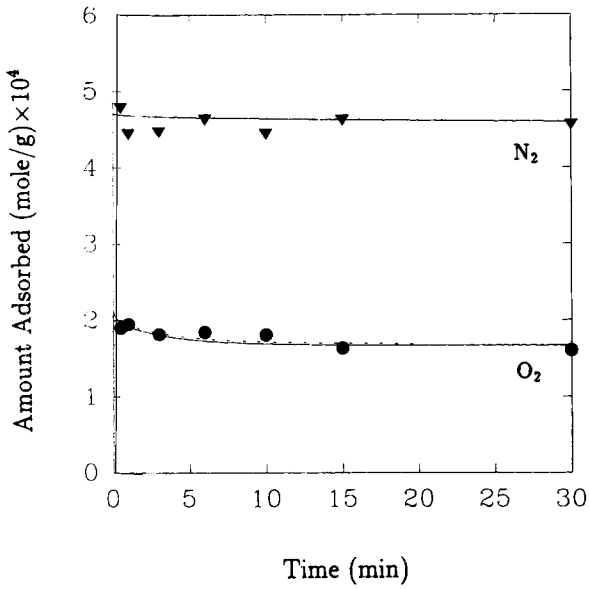

Figure 10. Codiffusion of N_2 and O_2 in CMS at 27°C.

Symbols are experimental data. Curves are predictions using pure-component diffusivities (· · · ·) and theoretical binary diffusivities (——). See Table 3 for initial and final conditions.

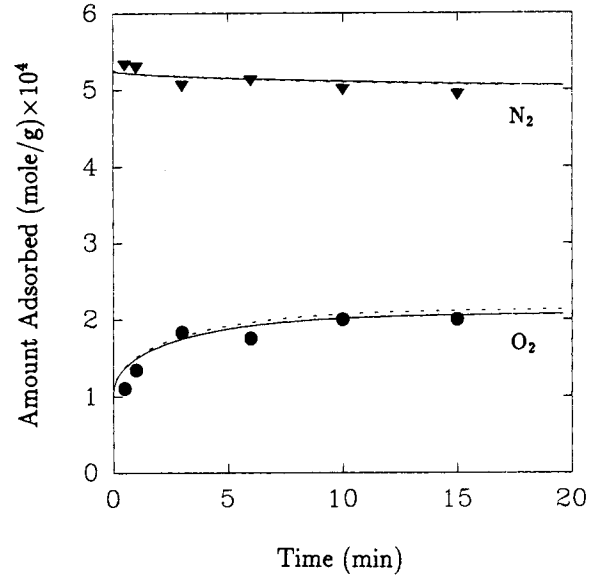

Figure 12. Counterdiffusion of N_2 and O_2 in CMS at 27°C.

Symbols are experimental data. Curves are predictions using pure-component diffusivities (· · · ·) and theoretical binary diffusivities (——). See Table 3 for initial and final conditions.

ures 9-14, as changes in adsorbate concentrations with time after the step change in the gas-phase composition.

To predict the binary uptake results, one needs to solve the binary Fickian diffusion equations:

$$\frac{\partial q_A}{\partial t} = \frac{1}{r^2}\frac{\partial}{\partial r}\left[r^2\left(D_{AA}\frac{\partial q_A}{\partial r} + D_{AB}\frac{\partial q_B}{\partial r}\right)\right] \tag{23}$$

$$\frac{\partial q_B}{\partial t} = \frac{1}{r^2}\frac{\partial}{\partial r}\left[r^2\left(D_{BA}\frac{\partial q_A}{\partial r} + D_{BB}\frac{\partial q_B}{\partial r}\right)\right] \tag{24}$$

with the initial and final adsorbate concentrations in Table 2. The crystals (or microparticles) are initially equilibrated (initial condition). The surface of the crystal is subjected to a step change as shown in Table 2, and the concentration gradient is zero at the center (two boundary conditions). The values of the four binary diffusivities are calculated from pure-component diffusivities based on the theory described above. The energy parameters used in the theoretical calculations are listed in Table 4. Equations 23 and 24 are solved numerically with the above boundary conditions and the predicted binary diffusivities. The predicted uptake curves are compared with the

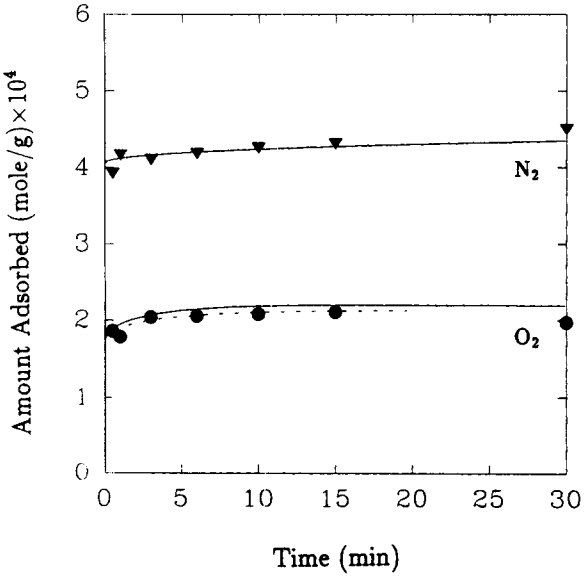

Figure 11. Codiffusion of N_2 and O_2 in CMS at 27°C.

Symbols are experimental data. Curves are predictions using pure-component diffusivities (· · · ·) and theoretical binary diffusivities (——). See Table 3 for initial and final conditions.

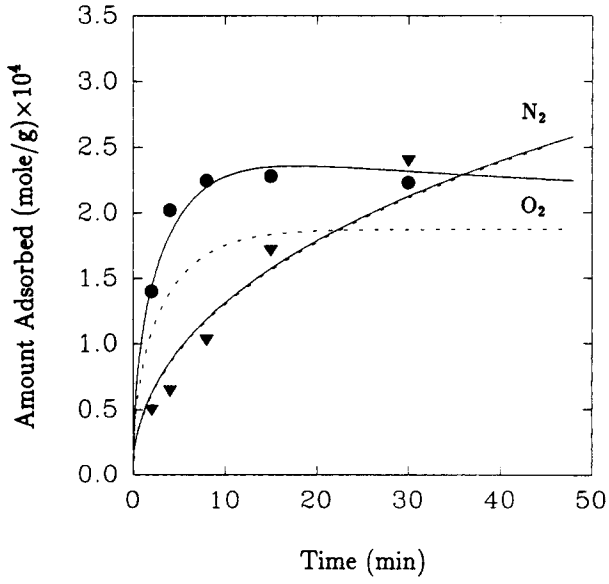

Figure 13. Codiffusion of N_2 and O_2 in CMS at 27°C.

Symbols are experimental data. Curves are predictions using pure-component diffusivities (· · · ·) and theoretical binary diffusivities (——). See Table 3 for initial and final conditions.

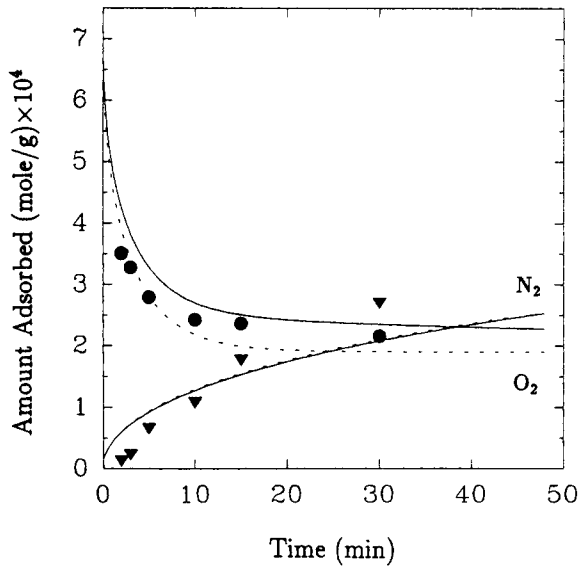

Figure 14. Counterdiffusion of N_2 and O_2 in CMS at 27°C.

Symbols are experimental data. Curves are predictions using pure-component diffusivities (· · · ·) and theoretical binary diffusivities (——). See Table 3 for initial and final conditions.

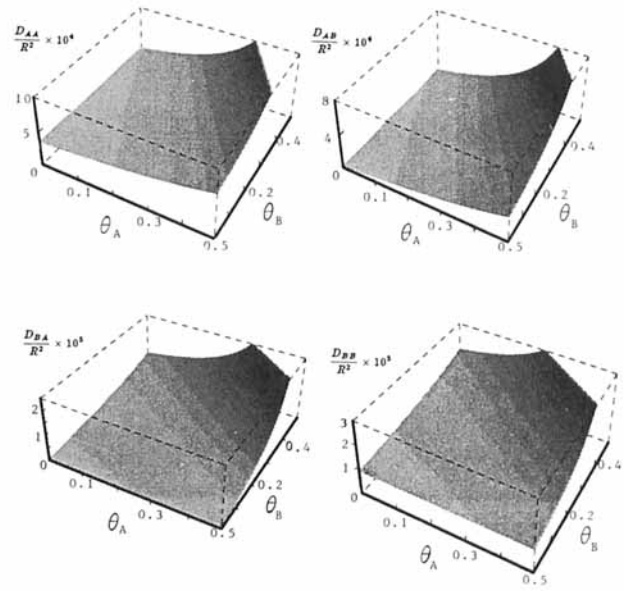

Figure 15. Dependence of binary diffusivities on fractional surface coverages (θ) for O_2 (A) and N_2 (B) in CMS at 27°C.

experimental data in Figures 9–14. Predicted curves are also calculated based on pure-component diffusivities. All diffusivities, both pure component and binary, are concentration-dependent. The predicted curves based on pure-component diffusivities are also shown in Figures 9–14 (dotted lines). In all figures, the predictions based on binary diffusivities seem to be in fair agreement with the experimental data. However, the best test of the binary theory predictions can be seen in Figure 13, where the deviations are the largest between the predictions based on binary and pure-component diffusivities, due to the large gradients imposed in the experiment. In this figure, the superiority of the binary theory is clearly demonstrated.

According to Eqs. 11–14, all four diffusivities are functions of θ_A and θ_B. The functional dependence is shown in Figure 15. Since the values of λ are small, all D values are positive. However, when $\lambda_{AB}>1$, D_{AB} will have a negative value (Eq. 12), and when $\lambda_{BA}>1$, D_{BA} will be negative (Eq. 13). Negative cross-term diffusivities have indeed been reported as discussed by Yang et al. (1991).

The experimental results show, as also predicted by the theory, that the fast diffusing species is more strongly affected than the slow diffusing species by the binary diffusion effects. The theoretical predictions in Figure 15 clearly illustrate this point. The binary effects are reflected by the cross-term diffusivities, D_{AB} and D_{BA}. For the fast species (species A), D_{AB} is quite significant as compared to D_{AA}. Whereas for the slow species (B), D_{BA} is not significant as compared to D_{BB} except for very high coverages. This phenomenon can also be understood from the following intuitive explanation. The binding energy (to surface sites) is stronger for the slow species, so its holding time is longer. Consequently, the binary effects are felt more strongly by the fast species.

Acknowledgment

This work was supported by NSF Grant CTS-9212279 and, in part, by the Donors to the Petroleum Research Fund administered by the American Chemical Society. A good description for the cross-term effects is "diffusive entrainment" by Nelson and Wei (1992).

Notation

a = radius of microparticle (crystal)
a_o = geometric mean radius on a volume fraction basis
a_o' = geometric mean radius on a number fraction basis
b = Langmuir constant
D = Fickian diffusivity
D_o = Fickian diffusivity at zero surface coverage
H = heat of adsorption
J = flux
n = number of components
P = pressure
q = amount adsorbed
q_s = saturated amount adsorbed
r = radial distance
R = radius microparticle (crystal) or gas constant
t = time
T = absolute temperature
x = distance
X = adsorbed-phase mole fraction

Table 4. Energy Parameters Used for Predicting Binary Diffusivities

ϵ_{AV} (kcal/mol)	ϵ_{BV} (kcal/mol)	ϵ_{AA} (kcal/mol)	ϵ_{BB} (kcal/mol)	$\epsilon_{AB}=\epsilon_{BA}$ (kcal/mol)	λ_{AB}	λ_{BA}
5.585	6.851	3.832	4.256	4.038	7.47×10^{-2}	8.93×10^{-3}

A = Oxygen; B = Nitrogen

Greek letters

ϵ = effective bond energy
ϵ_{AB} = heat of adsorption of A on site covered by B
ϵ_{Ai} = heat of adsorption
θ = surface coverage defined by $\theta = q/q_s$ or Eq. 17
σ = geometric standard deviation
λ = diffusional interaction, defined by Eqs. 18-21

Subscripts

A, B = components ($A = O_2$, $B = N_2$)
i, j = components
V = vacant site

Literature Cited

Carlson, N. W., and J. S. Dranoff, "On the Adsorption of Ethane by 4A Zeolite Pellets," *Ind. Engng. Chem. Process Des. Dev.*, **24**, 1300 (1985).

Carlson, N. W., and J. S. Dranoff, "Competitive Adsorption of Methane and Ethane on 4A Zeolite," *Fundamentals of Adsorption*, A. L. Liapis, ed., Engineering Foundation, New York (1987).

Chen, Y. D., and R. T. Yang, "Predicting Binary Fickian Diffusivities from Pure-component Fickian Diffusivities for Surface Diffusion," *Chem. Eng. Sci.*, **47**, 3895 (1992).

Chen, Y. D., R. T. Yang, and L. M. Sun, "Further Work on Predicting Multi-component Diffusivities from Pure-component Diffusivities for Surface Diffusion and Diffusion in Zeolites," *Chem. Eng. Sci.*, **48**, 2815 (1993).

Chihara, K., M. Suzuki, and K. Kawazoe, "Adsorption Rate on Molecular Sieving Carbon by Chromatography," *AIChE J.*, **24**, 237 (1978).

Do, D. D., X. Hu, and P. L. J. Mayfield, "Multicomponent Adsorption of Ethane, n-Butane and n-Pentane in Activated Carbon," *Gas Sep. Purif.*, **5**, 35 (1991).

Dominguez, J. A., D. Psaras, and A. I. LaCava, "Langmuir Kinetics as an Accurate Simulation of the Rate of Adsorption of Oxygen and Nitrogen Mixtures on Non-Fickian Carbon Molecular Sieves," *AIChE Symp. Ser.*, **84**(264), 73 (1988).

Farooq, S., and D. M. Ruthven, "Numerical Simulation of a Kinetically Controlled Pressure Swing Adsorption Bulk Separation Process Based on a Diffusion Model," *Chem. Eng. Sci.*, **46**, 2213 (1991).

Habgood, H. W., "The Kinetics of Molecular Sieve Action. Sorption of Nitrogen-Methane Mixtures by Linde Molecular Sieve 4A," *Can. J. Chem.*, **36**, 1384 (1958).

Irani, R. R., and C. F. Callis, *Particle Size: Measurement, Interpretation and Application*, Wiley, New York (1963).

Karger, J., and M. Bulow, "Theoretical Prediction of Uptake Behavior in Adsorption of Binary Gas Mixtures Using Irreversible Thermodynamics," *Chem. Eng. Sci.*, **30**, 893 (1975).

Karger, J., M. Bulow, and W. Schirmer, "Zur Adsorptionskinetik Von Binaren n-paraffin-benzol-gemischen an Synthetischen Zeolithen," *Z. Phys. Chemie., Leipsiz*, **256**, 144 (1975).

Karger, J., and H. Pfeifer, "NMR Self-diffusion Studies in Zeolite Science and Technology," *Zeolites*, **7**, 90 (1987).

Kawazoe, K., M. Suzuki, and K. Chihara, "Chromatographic Study of Diffusion in Molecular Sieve Carbon," *J. Chem. Eng. Japan*, **7**, 151 (1974).

Kikkinides, E. S., and R. T. Yang, "Concentrating CO_2 from Flue Gas by Pressure Swing Adsorption," *Ind. Eng. Chem. Res.*, **32**, 2714 (1993).

Knoblauch, K., "Pressure Swing Adsorption: Geared for Small Volume Users," *Chem. Eng.*, **85**, 87 (1978).

Krishna, R., "Problems and Pitfalls in the Use of the Fick Formulation for Intraparticle Diffusion," *Chem. Eng. Sci.*, **48**, 845 (1993).

LaCava, A. I., J. Dominguez, and J. Cardenas, "Modeling and Simulation of Rate Induced PSA Separation," *Adsorption: Science and Technology*, A. E. Rodrigues, M. D. LeVan and D. Tondeur, eds., Kluwer Academic Publishers, Boston (1989).

Ma, Y. H., and T. Y. Lee, "Diffusion of Binary Gas Mixtures in Zeolite X Pellets," *Ind. Eng. Chem. Fundam.*, **16**, 44 (1977).

Ma, Y. H., and A. J. Roux, "Multicomponent Rates of Sorption of SO_2 and CO_2 in Sodium Mordenite," *AIChE J.*, **19**, 1055 (1973).

Marutovsky, R. M., and M. Bulow, "Calculation of the Straight and Cross Diffusion Coefficients of a Two-Component Mixture in a Microporous Zeolitic Structure," *Zeolites*, **7**, 111 (1987).

Nelson, P. H., and J. Wei, "A Theory for Two-Component Diffusion in Zeolite," *J. Catal.*, **136**, 263 (1992).

Palekar, M. G., and R. A. Rajadhyaksha, "Sorption in Zeolites—III. Binary Sorpiton," *Chem. Eng. Sci.*, **41**, 463 (1986).

Qureshi, W. R., and J. Wei, "One- and Two-Component Diffusion in Zeolite ZSM-5: I. Theory," *J. Catal.*, **126**, 126 (1990).

Qureshi, W. R., and J. Wei, "One- and Two-Component Diffusion in Zeolite ZSM-5, II. Experimental," *J. Catal.*, **126**, 147 (1990b).

Ruthven, D. M., "Diffusion of Oxygen and Nitrogen in Carbon Molecular Sieve," *Chem. Eng. Sci.*, **47**, 4305 (1992).

Ruthven, D. M., and R. Kumar, "A Chromatographic Study of the Diffusion of N_2, CH_4 and Binary CH_4-N_2 Mixtures in 4A Molecular Sieves," *Can. J. Chem. Eng.*, **57**, 342 (1979).

Ruthven, D. M., N. S. Raghavan, and M. M. Hassan, "Adsorption and Diffusion of Nitrogen and Oxygen in a Carbon Molecular Sieve," *Chem. Eng. Sci.*, **41**, 1325 (1986).

Tsikoyiannis, J. G., and J. Wei, "Diffusion and Reaction in High-Occupancy Zeolite Catalysts: I. A Stochastic Theory," *Chem. Eng. Sci.*, **46**, 233 (1991a).

Tsikoyiannis, J. G., and J. Wei, "Diffusion and Reaction in High-Occupancy Zeolite Catalysts: II. Experimental Results," *Chem. Eng. Sci.*, **46**, 255 (1991b).

Walker, P. L. Jr., F. Rusinko, Jr., and L. G. Austin, "Gas Reactions of Carbon," *Adv. Catal.*, **11**, 133 (1959).

Yang, R. T., *Gas Separation by Adsorption Processes*, Butterworth, Boston (1987).

Yang, R. T., Y. D. Chen, and Y. T. Yeh, "Prediction of Cross-Term Coefficients in Binary Diffusion: Diffusion in Zeolite," *Chem. Eng. Sci.*, **46**, 3089 (1991).

Yang, R. T., J. B. Fenn, and G. L. Haller, "Modification on the Higashi Model for Surface Diffusion," *AIChE J.*, **19**, 1052 (1973).

Yasuda, Y., and K. Matsumoto, "Straight- and Cross-Term Diffusion Coefficients of a Two-Component Mixture in Micropores of Zeolites by Frequency Response Method," *J. Phys. Chem.*, **93**, 3195 (1989).

Manuscript received May 24, 1993, and revision received Aug. 16, 1993.